Arctic sea ice velocity field: General circulation and turbulent-like fluctuations

Pierre Rampal, Jérôme Weiss, David Marsan, Mickaël Bourgoin

JOURNAL OF GEOPHYSICAL RESEARCH, VOL. 114, C10014, doi:10.1029/2008JC005227, 2009

Arctic sea ice velocity field: General circulation and turbulent-like fluctuations

P. Rampal,[1,2] J. Weiss,[1] D. Marsan,[2] and M. Bourgoin[3]

Received 5 December 2008; revised 30 July 2009; accepted 14 August 2009; published 15 October 2009.

[1] Using buoy trajectories of the IABP data set, we analyze the Arctic sea ice velocity field as the superposition of a mean field and fluctuations. We study how the mean field can be objectively defined, using appropriate spatial and temporal averaging scales depending on the season considered: 400 km and 5 $^1/_2$ months for winter (i.e., approximately all the polar winter duration), and 200 km and 2 $^1/_2$ months for summer (i.e., approximately all the polar summer duration). The mean velocity field shows a strong intra-annual (between winter and the following summer) as well as interannual variability. The fluctuations, i.e., the remaining part of the velocity field after subtracting the mean field, are analyzed in terms of diffusion properties. Although the Arctic sea ice cover is a solid, we show that the fluctuations follow the same diffusion regimes as the ones predicted for turbulent flows, as observed in geophysical fluids like the ocean or the atmosphere. We found that the integral time and the diffusivity of sea ice are in the same ranges as those estimated for the ocean, i.e., 1.5 days in winter and 1.3 days in summer and 0.44×10^3 m^2/s for winter and 0.45×10^3 m^2/s in summer, respectively. However, the statistics of the sea ice fluctuating velocity deviate from classical turbulence theory, as they show exponential instead of Gaussian distributions. Sea ice velocity and acceleration are intermittent, and both are characterized by a multifractal scaling. The oceanic and atmospheric dynamic forcing cannot explain solely the statistical properties of sea ice kinematics and dynamics. We argue that sea ice dynamic is significantly influenced by the interplay of multiple fractures that are activated intermittently within the ice pack.

Citation: Rampal, P., J. Weiss, D. Marsan, and M. Bourgoin (2009), Arctic sea ice velocity field: General circulation and turbulent-like fluctuations, *J. Geophys. Res.*, *114*, C10014, doi:10.1029/2008JC005227.

1. Introduction

[2] "The motion of a particle of sea ice can be partitioned into a predictable component, associated with the long-term average wind and ocean currents, and a random part associated with the short-term fluctuations in the wind and current" [*Thorndike*, 1986a]. This citation suggests (1) the existence of a general circulation in the Arctic, and (2) that the random part simply results from ocean and atmosphere turbulence. Coming back to this problem, we here ask the following questions: (1) At which averaging scales (temporal & spatial) can we unambiguously define a general circulation of the Arctic sea ice? (2) What are the statistical properties of the fluctuating part of its motion? To what extent can we qualify the sea ice motion as being turbulent-like? (3) Can we see the fingerprint of oceanic and atmospheric forcing on these fluctuations?

[3] In order to investigate this problem, we develop an analogy with the approach used to study fluid turbulence and its associated diffusion properties. In fluid studies, the fluctuating part of the motion is commonly attributed to turbulence, and is distinguished from a predictable (in a deterministic sense) part, also called "mean flow". In other words, the Lagrangian or Eulerian velocities of parcels of a turbulent fluid are commonly separated into a mean velocity and its fluctuations (the so-called *Reynolds decomposition*) in order to characterize various turbulent properties of the fluid. Here we do the same for the Arctic sea ice velocities from a data set of buoy trajectories. Indeed, drifting buoys fixed to the sea ice cover were installed in the Arctic basin every year since 1978. These buoys can be considered as passive tracers (i.e., Lagrangian particles) of sea ice, like parcels would be for a fluid. The positions of the buoys that drifted according to sea ice motion, sometimes during more than one year, were recorded and made available by the International Arctic Buoy Program (IABP) (see section 2 for more details). These buoy trajectories show a pattern that looks like a "spaghetti" plot (see Figure 1). Similar patterns were observed for fluid parcels [*Bourgoin et al.*, 2006],

[1] Laboratoire de Glaciologie et Géophysique de l'Environnement, CNRS, Université Joseph Fourier, Saint Martin d'Hères, France.
[2] Laboratoire de Géophysique Interne et Tectonophysique, CNRS, Université de Savoie, Le Bourget du Lac, France.
[3] Laboratoire des Ecoulements Géophysiques et Industriels, CNRS, Université Joseph Fourier et Institut National Polytechnique de Grenoble, Saint Martin d'Hères, France.

0148-0227/09/2008JC005227$09.00

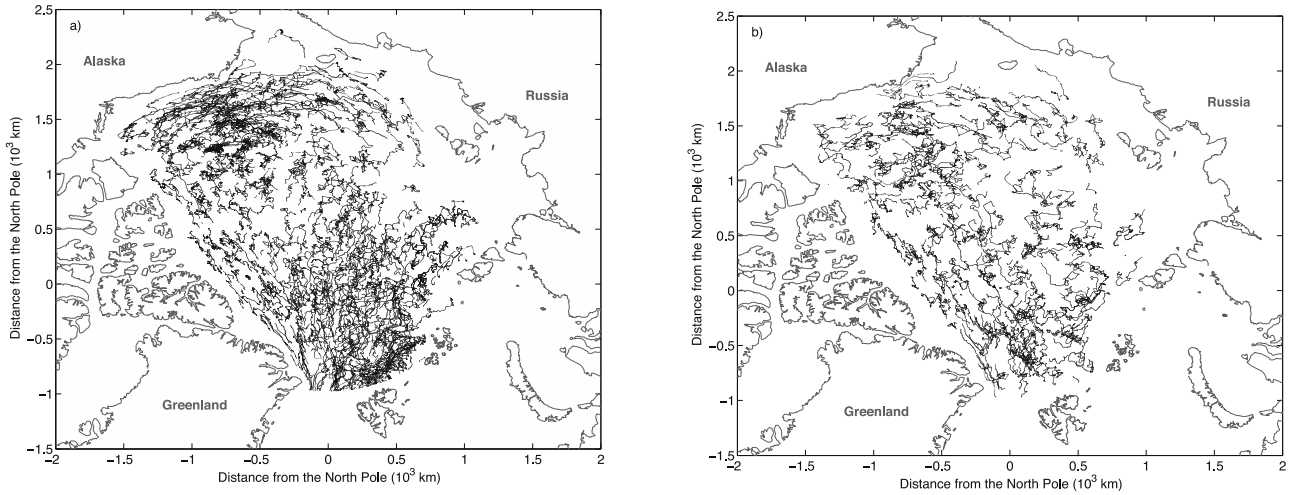

Figure 1. Map of the Arctic basin showing about 450 buoy tracks from the IABP data set for (a) winter and (b) summer. These trajectories were recorded between December 1978 and December 2001.

ocean surface drifters [*Haynes and Barton*, 1991; *Martins et al.*, 2002] or isopycnal floats [*Zhang et al.*, 2001], passively moving on in turbulent fluids. Like in all these cases, the motion of buoys appears to be forced by complex underlying processes.

[4] The possible analogy between sea ice motion and the motion of fluid parcels in a turbulent flow was remarkably introduced by *Thorndike* [1986a], who proposed a model that reproduces the mixing properties of the fluctuating velocity field. In another paper, *Colony and Thorndike* [1984] attempted to define the "Arctic mean general circulation" (AMGC). To do so, they estimated the mean field of sea ice motion using arbitrary spatial and temporal averaging scales of about 200 km and 90 years, from an interpolation (based on an optimal linear method [*Gandin*, 1963]) of about 100 trajectories recorded between 1893 and 1983. These averaging scales may not be appropriate: If the mean field of sea ice motion is estimated at too large spatial and/or temporal averaging scales, the homogenization will be too strong and small-scale details of the mean circulation will be lost. On the contrary, if the mean field is estimated at too small averaging scales, it will include a stochastic component coming from the fluctuating part of the motion, biasing the analysis of the velocity fluctuations as well as their causes (e.g., the forcing terms and the associated physical processes that are responsible for these fluctuations).

[5] The complexity of buoy trajectories suggests that sea ice velocities locally deviate from the mean velocity field (i.e., associated to the AMGC) as they show sudden changes in direction and magnitude. One expects these velocity fluctuations to result from different forcing terms. In the central Arctic region, and during the summer season, the sea ice velocity fluctuations estimated by *Thorndike and Colony* [1982] seem to be highly correlated with fluctuations in the geostrophic wind. On the other hand, a large part of the velocity fluctuations in winter and near the coasts (i.e., within about 400 km from the coasts, according to these authors) seem to be unexplained by wind and/or current fluctuations [*Thorndike and Colony*, 1982]. This suggests that the unexplained motion could be also the fingerprint of sudden displacements due to the activation of fractures and faults within the sea ice pack that is associated to the intermittent sea ice cover deformation [*Rampal et al.*, 2008].

[6] In this paper, we thus propose an approach inspired from the study of fluid turbulence that allows defining the sea ice motion as a superposition of a mean motion and fluctuations from a methodology based on the stability of the lagrangian statistics. In section 2, we briefly present the data set that we used in this study. In section 3, we estimate the appropriate spatial and temporal averaging scales used to extract the mean pattern of sea ice motion (the AMGC). In section 4, we characterize the properties of the fluctuating part of the motion and we discuss these properties in terms of a turbulent-like signature. We conclude in section 5. This work differs from what was done in the 1980s by Thorndike and his colleagues as (1) the amount of buoy data is much larger here, (2) we propose a methodology based on a physical principle to separate the mean circulation from the fluctuating part of the sea ice motion and (3) we investigate the intermittency characterizing sea ice velocity.

2. Data Set: Lagrangian Trajectories of Buoys

[7] The drifting buoys data set is provided by the International Arctic Buoy Program (IABP) and is available on the Web (http://www.iabp.apl.washington.edu). We selected approximately 450 drifters deployed between 1979 and 2001 over the entire Arctic basin (see Figure 1). The selection is based on two criteria. The first is the quality of the data, i.e., in terms of duration and sampling regularity. The second criterion is based on the distance of the trajectories from the nearest coast: the positions recorded at a minimum distance of 100 km away from the coasts are selected. From the selected trajectories, we separate the positions recorded in winter (i.e., from the beginning of November to the middle of May of the following year) from those recorded in summer (from the middle of June to the middle of September). The buoy positions distributed by the IABP differ slightly from the true positions sampled by the buoys: The actual buoy's tracks are irregularly sampled through time, with a mean time interval of 1 hour. Errors on these positions range from 100 m to 300 m, depending on the type of the positioning

system embarked on the buoy [*Thomas*, 1999]. In order to obtain a more regular sampling, a cubic interpolation of the raw positions is first performed, before resampling these at 3-hour time intervals (see the IABP documentation for further details).

[8] The reference coordinate system used in this study is a Cartesian coordinate system centered on the North Pole with the vertical axis (i.e., the y axis) following the Greenwich meridian. Each latitude-longitude buoy position is expressed in the orthogonal base $(\mathbf{e}_1, \mathbf{e}_2)$ of this coordinate system as $\mathbf{x}_{(lat,long)} = x\mathbf{e}_1 + y\mathbf{e}_2$ using a polar stereographic projection. From the positions we compute the two components (i.e., along x axis and y axis) of the 3-hourly velocity vectors $\mathbf{u}$ as:

$$u_x(\tilde{x}, \tilde{t}) = (x(t + 3h) - x(t))/3h \tag{1}$$

$$u_y(\tilde{y}, \tilde{t}) = (y(t + 3h) - y(t))/3h \tag{2}$$

where $\tilde{x} = (x(t + 3h) + x(t))/2$, $\tilde{y} = (y(t + 3h) + y(t))/2$ and $\tilde{t} = ((t + 3h) + t)/2$. Positions uncertainties on the raw data give, after the cubic interpolation, an upper bound of the errors on the speed estimates ranging from 1.3 to 3 cm/s.

3. Estimating the Mean Velocity Field $\langle \mathbf{u}(\mathbf{x}, t) \rangle$ of the Arctic Sea Ice

[9] In this section, we quickly summarize the diffusion properties of a turbulent fluid (section 3.1), and more particularly, how a mean velocity field $\langle \mathbf{u}(\mathbf{x}, t) \rangle$ and its fluctuations $\mathbf{u}'(\mathbf{x}, t)$ (the so-called Reynolds decomposition) can be computed from Lagrangian velocities $\mathbf{u}(\mathbf{x}(t), t)$ records (section 3.2). To do so, the Lagrangian statistics of the fluctuating velocity field are first computed. These statistics are dependent on the partitioning of the velocity field, i.e., the spatial and temporal averaging scales chosen to estimate the mean field $\langle \mathbf{u}(\mathbf{x}, t) \rangle$ [*Bauer et al.*, 1998; *Zhang et al.*, 2001]. To determine the spatial and temporal averaging scales at which the partitioning should be performed, one has to consider the stability of the Lagrangian statistics with respect to these averaging scales. More particularly, we study the correlation properties of the fluctuating field (see section 3.2). This methodology is applied to the IABP buoy's trajectories in section 3.3. The results are presented in section 3.4. Using appropriate averaging scales deduced from this investigation, we compute examples of such mean velocity fields and we discuss their properties (see section 3.5).

3.1. Classical Approach: The Turbulent Diffusion Theory [*Taylor*, 1921]

[10] *Taylor* [1921] showed that in the case of a steady and homogeneous turbulence without mean flow, single-particle dispersion through time (i.e., the variance of the distance from its origin) $\langle r'^2(t) \rangle$ is related to the normalized turbulent autocorrelation function $C(\tau)$ as follows:

$$\langle r'^2(t) \rangle = 2\Gamma \langle u'^2 \rangle \int_0^t C(\tau) d\tau \tag{3}$$

where $\langle u'^2 \rangle$ is the fluctuating speed variance and Γ is the so-called integral time [*Taylor*, 1921]. The turbulent autocorrelation function $C(\tau)$ is defined as follows:

$$C(\tau) = \frac{1}{\langle u'^2 \rangle T_{\max}} \int_0^{T_{\max}} \mathbf{u}'(t)\mathbf{u}'(t + \tau) dt \tag{4}$$

where $T_{\max}$ is the maximum time of data coverage and $\mathbf{u}'$ is the fluctuating velocity defined as $\mathbf{u}' = \mathbf{u} - \langle \mathbf{u} \rangle$. Theoretically, $C(\tau)$ decreases with increasing time lag (e.g., following an exponential decay) as particles loose the memory of their previous displacements past a characteristic memory time Γ [*Taylor*, 1921] defined as:

$$\Gamma = \int_0^\infty C(\tau) d\tau \tag{5}$$

We denote Λ as the translation in the spatial domain of the integral time Γ. Λ is commonly estimated as $\Lambda = \langle u'^2 \rangle^{1/2} \Gamma$ [*Frisch*, 1995]. From equations (3) and (5), we deduce that particle dispersion $\langle r'^2(t) \rangle$ has two asymptotic regimes. For $t \ll \Gamma$, one obtains:

$$\langle r'^2(t) \rangle \sim t^2 \tag{6}$$

that is, the variance of the turbulent displacement grows with t^2. This is the so-called "ballistic" regime or "initial growth" stage. For $t \gg \Gamma$, one obtains:

$$\langle r'^2(t) \rangle \sim \Gamma t \tag{7}$$

that is, the variance of the turbulent displacement grows with t, i.e., like single-particle dispersion for molecular diffusion. This regime is the direct consequence of (1) the Gaussian statistics of the turbulent speed and (2) the fact that, at $t \gg \Gamma$, the velocity correlations vanish. The Lagrangian turbulent diffusivity K provides a measure of the rate of spreading of a particle from its initial position, which gives the rate of change of the root mean square particle position relative to the mean trajectory of the particle:

$$K = \frac{1}{2} \frac{d\langle r'^2(t) \rangle}{dt} \tag{8}$$

From equations (7) and (8), one obtains that for $t \ll \Gamma$,

$$K = \langle u'^2 \rangle t \tag{9}$$

and for $t \gg \Gamma$,

$$K = \langle u'^2 \rangle \Gamma \tag{10}$$

A complementary description of this theory in the context of oceanic drifters can be found in *Zhang et al.* [2001].

3.2. Definition of the Mean Velocity $\langle \mathbf{u} \rangle$

[11] In his theory, *Taylor* [1921] considers the turbulent velocity $\mathbf{u}'$ of a flow. The turbulent velocity is deduced by

subtracting the mean velocity $\langle \mathbf{u} \rangle$ from the velocity $\mathbf{u}$. The question is this: How do we compute the mean?

[12] When Lagrangian observers (mainly drifters and floats) were first used in ocean observations, they were used in such limited numbers that it was necessary to estimate and use a constant mean velocity over the whole observational domain [*Freeland et al.*, 1975; *Riser and Rossby*, 1983; *Colin de Verdière*, 1983; *Sundermeyer and Price*, 1998]. As the number of observations increased, it was possible to resolve, to a limited extent, the spatial variations of the mean flow, say by binning observational data in large boxes [*Krauss and Böning*, 1987; *Spall et al.*, 1993; *Poulain et al.*, 1996]. This is an improvement over the uniform mean flow, but in strong current regions the data density is not high enough to extract details of the highly structured mean flow.

[13] More generally, we denote by $\langle \mathbf{u}(\mathbf{x}, t) \rangle_{L,T}$ the Eulerian velocity field smoothed at spatial and temporal scales L and T:

$$\langle \mathbf{u}(\mathbf{x}, t) \rangle_{L,T} = \int \int \Phi_{L,T}(\mathbf{x} - \mathbf{x}', t - t') \mathbf{u}(\mathbf{x}', t') dt' d\mathbf{x}' \qquad (11)$$

where $\Phi_{L,T}(\mathbf{x}, t)$ is a smoothing kernel with the two characteristic scales L and T. Here the mean $\langle \mathbf{u} \rangle_{L,T}$, and consequently its associated fluctuation $\mathbf{u}'$, depend on the choice of L and T.

[14] *Zhang et al.* [2001] and *Bauer et al.* [1998] studied the influence of L on the Lagrangian statistics of oceanic currents (the North Atlantic Current region and the tropical Pacific Ocean, respectively) from float data sets. For example, taking the largest temporal window allowed by their data set for T (i.e., 2 years) and L (i.e., the length of box side) ranging from 0.3° to 4°, *Zhang et al.* [2001] found a strong dependence of (1) the turbulent velocity variance, (2) the integral time Γ, (3) the integral length Λ and (4) the turbulent diffusivity K, on the spatial averaging scale L. Nevertheless, above a threshold value $\tilde{L} = 0.5°$, they observed that these statistics remained constant. In the works of *Zhang et al.* [2001] and *Bauer et al.* [1998], such saturation in the Lagrangian statistics is interpreted as the fact that an averaging of Lagrangian velocities at the scale $\tilde{L}$ allows to correctly resolve the spatial structure of the mean flow, i.e., avoids to embed in the residual turbulent field the unresolved mean velocity structure.

[15] To further illustrate this point, and introduce in the same time our following analysis, let us consider a set of about 30 trajectories from the IABP data set. This set corresponds to all the positions of 30 buoys recorded between the beginning of December 1992 and the end of October 1993. From their 3-hourly Lagrangian velocities $\mathbf{u}(\mathbf{x}(t), t)$, we estimate at each position $\mathbf{x}$ of all the 30 buoys the mean velocity noted $\langle \mathbf{u}(\mathbf{x}(t), t) \rangle_{L,T}$ by averaging their velocities over different couples of spatial and temporal scales (L, T) (see section 3.3 for a complete description of the mean estimation methodology). Then, we calculate the local fluctuating velocity as:

$$\mathbf{u}'(\mathbf{x}(t), t) = \mathbf{u}(\mathbf{x}(t), t) - \langle \mathbf{u}(\mathbf{x}(t), t) \rangle_{L,T} \qquad (12)$$

Figure 2 displays the displacements $r'(t)$ of each buoy due to the local fluctuating velocity $\mathbf{u}'(\mathbf{x}, t)$ computed following equation (12) for different scales (L, T). Looking at the size of the region containing the displacements $r'(t)$, we can, at least graphically, estimate in this simple example the integral length Λ. We estimate Λ as being the radius of the smallest circle containing all the fluctuation trajectories. Λ corresponds to a characteristic length scale, e.g., a characteristic size of structure. We can deduce from Figure 2 that Λ (and thus Γ) increases with L and T until a maximum is reached for L and T of about 400 km and 160 days (i.e., 5 $^1/_2$ months) approximately. Thus by averaging at these scales, no spatial and/or temporal correlations inherent to the fluctuating velocity field remain in the mean field. In other words, the mean velocity field can be considered as homogeneous and stationary [*Figueroa and Olson*, 1994], i.e., the diffusion follows the theory of *Taylor* [1921]. We conclude that these scales are appropriate to estimate the mean and therefore also the fluctuating velocity fields. Another interesting remark is that despite the asymmetry of the actual trajectories, the fluctuating trajectories are symmetric, i.e., the fluctuating displacements are approximately isotropic around the reference point (0, 0) in Figure 2.

[16] Hereafter, we study the influence of the choice of the averaging scales on the integral time Γ defined in equation (5) for the entire IABP data set, in order to find the smallest averaging scales $\tilde{L}$ and $\tilde{T}$ (i.e., the highest resolution for the Eulerian mean field) above which Γ remains essentially unchanged.

3.3. Methodology

[17] Let us index by q the buoys of our data set ($1 < q < N$). N is the total number of the selected buoys trajectories, i.e., approximately 350 in winter and 230 in summer. For each position $\mathbf{x}_{ref}$ reached at time t_{ref} by the drifting buoy q, we estimated the mean velocity $\langle \mathbf{u}(\mathbf{x}_{ref}, t_{ref}) \rangle_{L,T}$. To do this, for each location ($\mathbf{x}_{ref}$, t_{ref}) we selected in our data set all n velocity vectors $\mathbf{u}_k$ ($1 < k < n$) situated in a circle of diameter L centered on $\mathbf{x}_{ref}$ and in a temporal window of duration T centered on t_{ref}.

[18] This simple averaging faces an estimation problem: Let us sort the n velocity such that their separations r_k from $\mathbf{x}_{ref}$ are in ascending order. We denote the velocity vectors and their corresponding separations as $\mathbf{u}_i$ and r_i, respectively, where index i is such that $r_1 < r_2 < \ldots < r_n$. If these n vectors were densely spaced around $\mathbf{x}_{ref}$, the cumulative number of velocity vectors noted $N(<r)$ situated within the circle of radius r centered on $\mathbf{x}_{ref}$ would increase as r^2. Looking at the evolution of the rank i as a function of r_i, we checked for a particular example that $N(<r_i) \sim r_i^d$ with $d < 2$ and that d decreases with L decreasing (see Figure 3), i.e., the dense repartition hypothesis is less and less true as one decreases the spatial scale of observation. This can be understood as the result of a spatial heterogeneity of the data due to the fact that (1) a significant part of the n-vectors belongs to the same buoy q considered, and (2) some sets of buoys were launched at the same time in the vicinity of each others (i.e., "bunch" launches). The mean velocity computed from the n vectors matching a spatial window of scale L would then be biased if we use a uniform weighting, as we would give too much weight to the velocity vectors situated in the vicinity

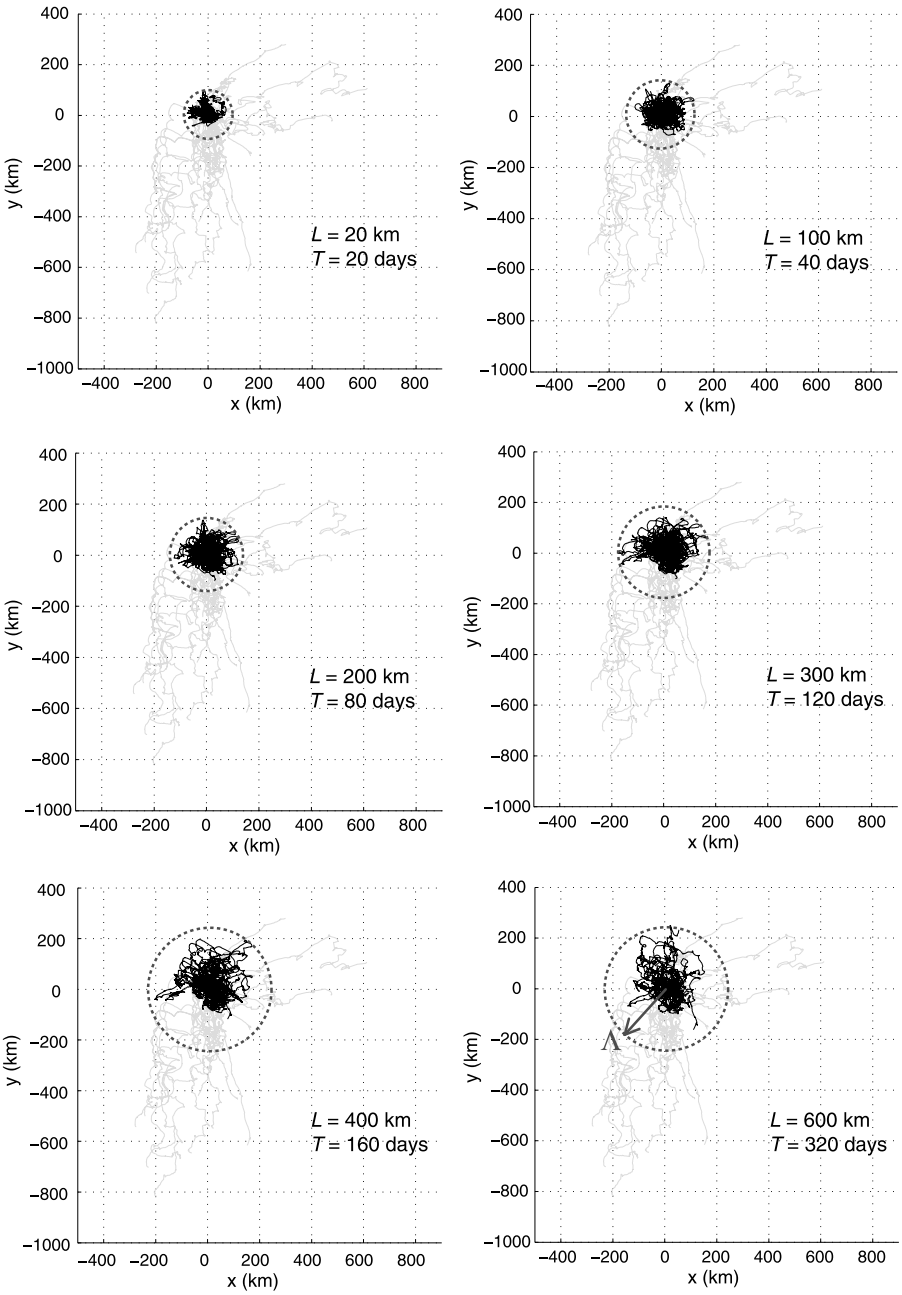

Figure 2. Displacements fluctuations $r'(t)$ (in black) of buoys that worked during the winter 1992–1993 (i.e., 30 trajectories). These displacements are linked to the fluctuating velocity field deduced from mean velocity fields estimated at different scales (L, T). The actual displacements $r(t)$ of the buoys are drawn in gray. The initial positions of the fluctuating (i.e., $\mathbf{x}'(t = 0)$) as well as the actual trajectories (i.e., $\mathbf{x}(t = 0)$) of each buoy have been set to (0, 0). Looking at the size of the region containing the displacements $r'(t)$ (marked as the dashed gray circles), we can see the dependence of the integral length Λ on the spatial and temporal averaging scales.

of $\mathbf{x}_{ref}$. So we took into account for this effect in the weights calculation by computing a correcting term w_i^c associated to each velocity vector $\mathbf{u}_i$ and corresponding to the deviation of $N(<r_i)$ from r_i^2 as $w_i^c = r_i^2/i$.

[19] Let us go back now to the mean calculation. For each velocity $\mathbf{u}_k$, we computed the weighting coefficient w_k depending on (1) the separation $r_k = \|\mathbf{x}_{ref} - \mathbf{x}_k\|$, (2) the time lag $\tau_k = |t_{ref} - t_k|$ and (3) the bias due to spatial heterogeneity w_i^c as follows:

$$w_k = w_i^c e^{\left(-\frac{r_k^2}{2L^2} - \frac{\tau_k^2}{2T^2}\right)} \tag{13}$$

The reason behind the particular format of equation (13) is that we consider Gaussian kernels in time and space in our

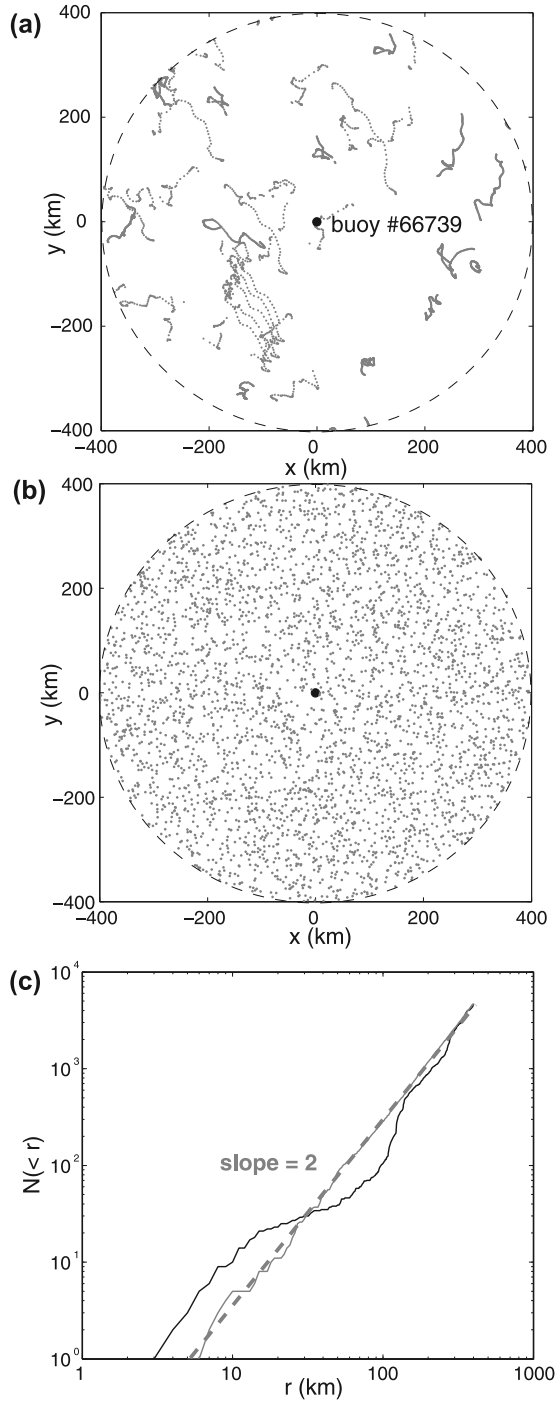

Figure 3. Illustration of the spatial heterogeneity of the buoy positions available during any calendar month of January between 1979 and 2007. Here the position of the buoy 66737 recorded on 13 January 2007 is set as the reference position. (a) The 4630 buoy positions found in the January months of 1979–2007 plotted within 400 km of the reference position. This can be compared to (b) a set of 4630 synthetic positions computed following a Poisson distribution. (c) Number $N(<r)$ of positions contained in the disk of radius r centered on (0,0) for actual buoy positions (dark line) and synthetic positions (gray line). $N(<r)$ follows a r^2 law (gray dashed line) for the Poisson distribution. For IABP buoys, $N(<r)$ deviates from this law. The term w^c in equation (13) is introduced to correct for this effect.

weight calculation, i.e., the function $\Phi_{L,T}$ of equation (11) is taken as Gaussian. We computed the mean velocity associated to the buoy q at location $(\mathbf{x}_{ref}, t_{ref})$ for the averaging scales L and T as:

$$\left\langle \mathbf{u}\left(\mathbf{x}_{ref},t_{ref}\right)\right\rangle_{L,T}=\frac{1}{\sum\limits_k w_k}\sum_k w_k\mathbf{u}_k \tag{14}$$

We deduced from the mean $\langle \mathbf{u}(\mathbf{x}_{ref}, t_{ref})\rangle_{L,T}$ the fluctuating velocity of the buoy q as $\mathbf{u}'_q(\mathbf{x}_{ref}, t_{ref}) = \mathbf{u}_q(\mathbf{x}_{ref}, t_{ref}) - \langle \mathbf{u}(\mathbf{x}_{ref}, t_{ref})\rangle_{L,T}$. Then, we computed the normalized autocorrelation (i.e., the linear correlation coefficient) functions $C_q^{L,T}(\tau)$ of $\mathbf{u}'_q$ following equation (4) for L and T varying from 20 to 600 km and from 10 to 240 days respectively, and for τ ranging from 0 to 20 days by steps of 3 hours. The ensemble average autocorrelation function $\chi^{L,T}(\tau)$ was obtained by averaging over all the trajectories available:

$$\chi^{L,T}(\tau)=\left\langle C_q^{L,T}(\tau)\right\rangle=\frac{1}{\sum\limits_q T^q_{\max}}\sum_q T^q_{\max}C_q^{L,T}(\tau) \tag{15}$$

$T^q_{\max}$ is the time interval during which the buoy q worked. We checked that our functions $\chi^{L,T}(\tau)$ tends to zero in a finite time and that we can define the integral timescale $\Gamma^{L,T}$ (see section 4.1 for further details). However, the finite length of the time series of buoy's positions leads to problems when determining the integral timescale $\Gamma^{L,T}$ using equation (5), since we cannot integrate to infinity. The usual practice is to integrate $\chi(\tau)$ from zero to the time of the first zero crossing, also called the "time of integration". This corresponds to the first maximum of the integral scale and the result obtained can be regarded as an upper bound to the true scale [*Poulain and Niiler*, 1989]. Consequently, we estimate the integral timescale $\Gamma^{L,T}$ associated to each correlation function $\chi^{L,T}(\tau)$ following equation (5) as

$$\Gamma^{L,T}=\int_0^{t_0}\chi^{L,T}(\tau)d\tau \tag{16}$$

where t_0 is the time of integration. Finally, we search for the lower bound space-time scales $(\tilde{L}, \tilde{T})$ of averaging above which $\Gamma(L, T)$ remains quasi constant, i.e., admitting less than 1% of change from $\Gamma(\tilde{L}, \tilde{T})$.

3.4. Results and Conclusions

[20] Figure 4 shows the autocorrelation functions $\chi^{L,T}(\tau)$ computed for the winter data set and for three different cases: when no mean field is removed, when the mean field calculated for L = 50 km and T = 40 days is removed, and when the mean field calculated for L = 400 km and T = 160 days is removed. When no mean field is removed from the original signal, the autocorrelation function never crosses zero and stabilizes around 0.05, i.e., a residual correlation persists after 20 days. This is the mark of the predictable character, in the deterministic sense, of the mean circulation. For spatial and temporal averaging scales below 400 km and 160 days respectively, the autocorrelation function shows negative values until approximately 20 days. This is due to the fact that for these averaging scales we

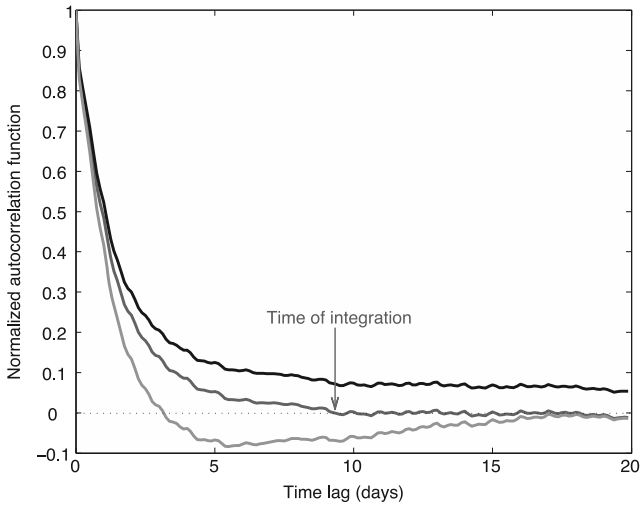

Figure 4. Normalized autocorrelation functions of fluctuating velocity. The fluctuating velocities are calculated after removing the mean velocity field estimated for different averaging spatial and temporal scales: no mean flow removed (in dark), the removed mean velocity field computed for L = 50 km and T = 40 days (in light gray), and for L = 400 km and T = 160 days (in dark gray). We define the time of integration t_0 for the last two cases as the time of the first zero crossing.

artificially include in the computed mean field some spatial and temporal variability that is not deterministic, i.e., a random part of the motion. By doing so, we remove this variability from the fluctuating velocity field and then we bias the associated autocorrelation function. For spatial and temporal averaging scales larger than 400 km and 160 days, the autocorrelation function stabilizes, as expected. However, using such averaging scales, one would loose information about the details of the mean circulation.

[21] We show in Figure 5 the Γ values deduced from the autocorrelation functions $\chi^{L,T}(\tau)$ for winter. For scales under 400 km and 160 days, the Γ value increases strongly (i.e., from 0.6 to 1.4 days) with increasing averaging scales. Above these lower bounds, the function $\Gamma_{win}(L, T)$ reaches a plateau around 1.5 days (the relative variation of Γ is lower than 1%). This is the confirmation of what we deduced from the analysis of the autocorrelation functions. Symmetrically, we find that Λ reaches a plateau around 20 km.

[22] Thus we conclude that the appropriate averaging scales to compute the AMGC for winter are $\tilde{L}$ = 400 km and $\tilde{T}$ = 160 days, i.e., approximately one winter in the polar season. For summer, we find that (1) the function $\Gamma(L, T)$ reaches a plateau around 1.3 days and (2) the appropriate averaging scales are $\tilde{L}$ = 200 km and $\tilde{T}$ = 80 days, i.e., approximately one summer in the polar season. As a comparison, *Colony and Thorndike* [1984] and *Thorndike* [1986b] estimated the integral timescale of sea ice motion from 28 trajectories of buoys that drifted in the Arctic basin during winter and/or summer, computing the time autocorrelation function for x and y components of the total velocity (i.e., without any mean removed), and found a value around 5 days. A simple view is that the 5-day timescale corresponds to atmospheric synoptic influences while our timescale corresponds to oceanic processes. This much larger value than the one we found illustrates the bias on the Lagrangian statistics that is obtained if no mean velocity is removed before the analysis, i.e., if the predictable part of the motion is kept. This points out the fact that it is crucial to (1) estimate unambiguously and then (2) remove the mean velocity field, in order to estimate correctly the properties of the fluctuating velocity field.

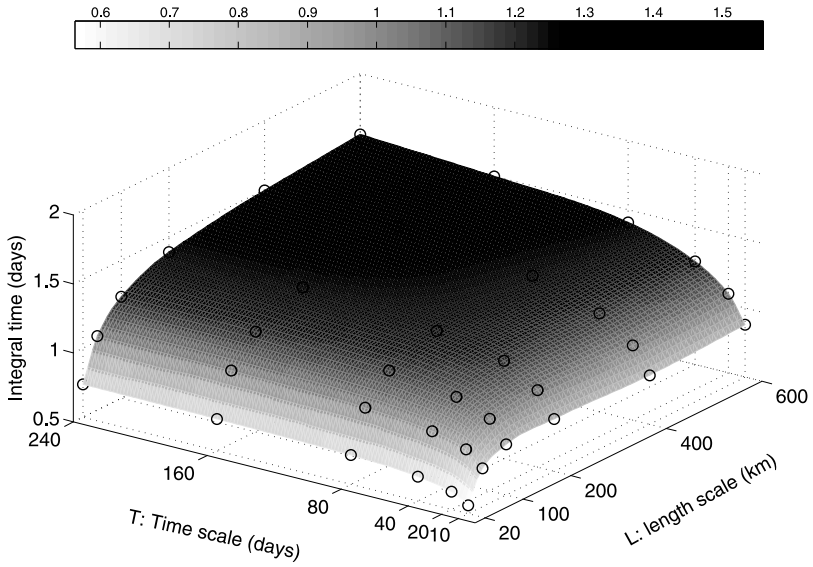

Figure 5. Integral timescale (i.e., Lagrangian time of correlation) for sea ice in winter versus the spatial and temporal scales at which the mean flow is estimated. The integral time is estimated from the Lagrangian autocorrelation functions by integrating between t = 0 and the time of integration t_0. The estimated integral times are drawn as light gray circles. The filled surface is the interpolated surface that shows a plateau for scales larger than 400 km and 160 days. At these scales the integral time is about 1.5 days and remains stable at larger scales.

3.5. Discussion

[23] To illustrate how such mean fields look like, we compute the mean velocity fields for the winters 1992/93 and 2000/01 and their respective following summers (i.e., the summers 1993 and 2001). These mean fields are interpolated on a regular grid of 400 km and 200 km respectively, following the appropriate averaging scales (see Figure 6). The errors $\Delta\overline{u}$ on the mean speed estimates $\overline{u}$ are estimated by using the central limit theorem, i.e., considering independent speed values. Two speed values are independent if (1) they are recorded by two different buoys separated by a distance $l \gg \Lambda$ (i.e., the integral length), or (2) if they are recorded by the same buoy with a time lag much larger than Γ (i.e., the integral time). These errors range from 4 to 25% for winter, and from 6 to 33% for summer. We can note here that despite the apparent large scales used for averaging, these mean fields contain exhaustive information on the predictable part of sea ice motion. On the winter 1992–1993 mean field map (Figure 6a), we can identify the Beaufort Gyre and the Transpolar Current, as found by *Colony and Thorndike* [1984] after averaging over 90 years. We checked that an average over all our data set gives a similar circulation pattern than the one of *Colony and Thorndike* [1984]. However, averaging over 90 years induces a lost of information about the interannual variability of the AMGC. This is confirmed by a look at the winter 2000–2001 mean field map (Figure 6b), where the mean field shows a different pattern: the center of the gyre is shifted through the West and the Transpolar Current appears less clearly. This interannual variability is illustrated in Figure 6c for which the difference between both winter mean fields is plotted. This plot shows that the difference in the velocity magnitudes can reach up to 4 cm/s in the Transpolar Current region, i.e., a value of the same order than typical velocity magnitudes observed for each winter. The mean speeds reached up to 6.8 cm/s in the Fram Strait for the winter 1992–1993 while they never exceed more than 5 cm/s for the winter 2000–2001. Almost null values are observed in the centre of the Beaufort Gyre for both winters. On the summer 1993 map (Figure 6d), the circulation draws quite a different picture compared to the previous winter (i.e., winter 1992–1993). Along with the Transpolar Drift, two independent gyres are revealed: the first one is a clockwise gyre centered on the north of the Beaufort basin and the second one is an anticlockwise gyre centered on the Laptev Sea. During this particular summer, the mean speeds reached up to 7.5 cm/s. Similarly to winters, the mean field of summer 2001 shows a different pattern than the one of 1993: The rotation of the gyre changed to anticlockwise. Its center shifted to the West, and was then located near the Transpolar Current region. The strong interannual variability of the velocity mean field for summer is illustrated on Figure 6f. Very strong differences in the velocity magnitudes are observed and range up to 7.8 cm/s. We also checked that the only perennial structure in the AMGC from one year to another is the Transpolar Drift.

[24] Thus there exists strong seasonal and interannual variability of the mean velocity field of sea ice. One could associate this variability to a change in the forcing, as atmospheric and/or oceanic conditions are known to change significantly from winter to summer, and from one year to another [*Thorndike and Colony*, 1982; *Hurrell*, 1995; *Thompson and Wallace*, 1998; *Rigor et al.*, 2000; *Overland et al.*, 2004; *Deser and Teng*, 2008]. It is worth noting here that this interannual variability has nothing to do with the stochastic fluctuations of the remaining part of the sea ice motion.

4. Analyzing the Fluctuating Velocity Field of Arctic Sea Ice

[25] Once a correct estimation of the mean velocity field of the Arctic sea ice is obtained, an analysis of the fluctuations can be performed. In the following, we describe the sea ice velocity fluctuations estimated for averaging scales $\tilde{L}$ and $\tilde{T}$ as established in section 3 (i.e., 400 km and 160 days for winter, and 200 km and 80 days for summer). In addition to the results of section 3, we here investigate other statistical properties of the sea ice velocity fluctuations and we compare them with those predicted by the turbulent diffusion theory of *Taylor* [1921].

4.1. Spectral Analysis

[26] Let us first come back on the autocorrelation function $\tilde{\chi}(\tau)$ defined as equation (15), focusing first on the winter season. It decreases as an exponential $\rho(\tau) \sim e^{-\tau/\tilde{\Gamma}}$ (with $\tilde{\Gamma} \approx 1.5$ days, see Figure 7), from the smallest timescales explored in our analysis (i.e., 3 hours) to $5\tilde{\Gamma}$ (see inset of Figure 7).

[27] Note that, as the variance of the autocorrelation function must be defined [*Voth et al.*, 1998], there has to be some lower cutoff to this behavior at time $\tau_\eta \ll 3$ hours [*Sawford*, 1991]. τ_η would then be for the sea ice motion a kind of turbulent-like dissipative scale. This point would be a subject for future investigations, requiring sea ice velocity measurements with much better spatial as well as temporal accuracy.

[28] We now turn to the Lagrangian spectrum, i.e., the power spectrum in time of the sea ice velocity fluctuations. We compute the Fourier transform $P(k)$ of the autocorrelation function $\tilde{\chi}(\tau)$ using a rectangular window as a smoothing filter. $P(k)$ is shown on Figure 8. For both winter and summer we observe a clear range of power law scaling $P(k) \sim k^{-2}$. Departure from the k^{-2} scaling is observed at low frequencies in agreement with the exponential decay of the autocorrelation. At high frequencies, the spectrum deviates from the k^{-2} scaling as the consequence of aliasing effects. Also, we checked that the Lagrangian spectrum of the velocity increments computed for a time range of 3 hours, which then approximates the Lagrangian spectrum of the acceleration [*Frisch*, 1995], is flat, as expected by the k^{-2} scaling of the sea ice velocity fluctuations. In other words, the Lagrangian acceleration of the fluctuating part of Arctic sea ice motion is uncorrelated in time (white noise), and can be therefore considered as a Markov process [*Sawford*, 1991].

[29] As a comparison with fluid turbulence, we note that such k^{-2} scaling coincides for example with the Kolmogorov K41 theoretical picture in which the spectral density at a frequency k is a dimensional function of k and of the dissipative rate of kinetic energy ε as $P(k) \propto \varepsilon k^{-2}$. Such k^{-2} scaling was reported for oceanic turbulence [*Lien et al.*, 1998] and atmospheric turbulence [*Gifford*, 1955; *Hay and Pasquill*, 1959; *Hanna*, 1980] in the Lagrangian framework.

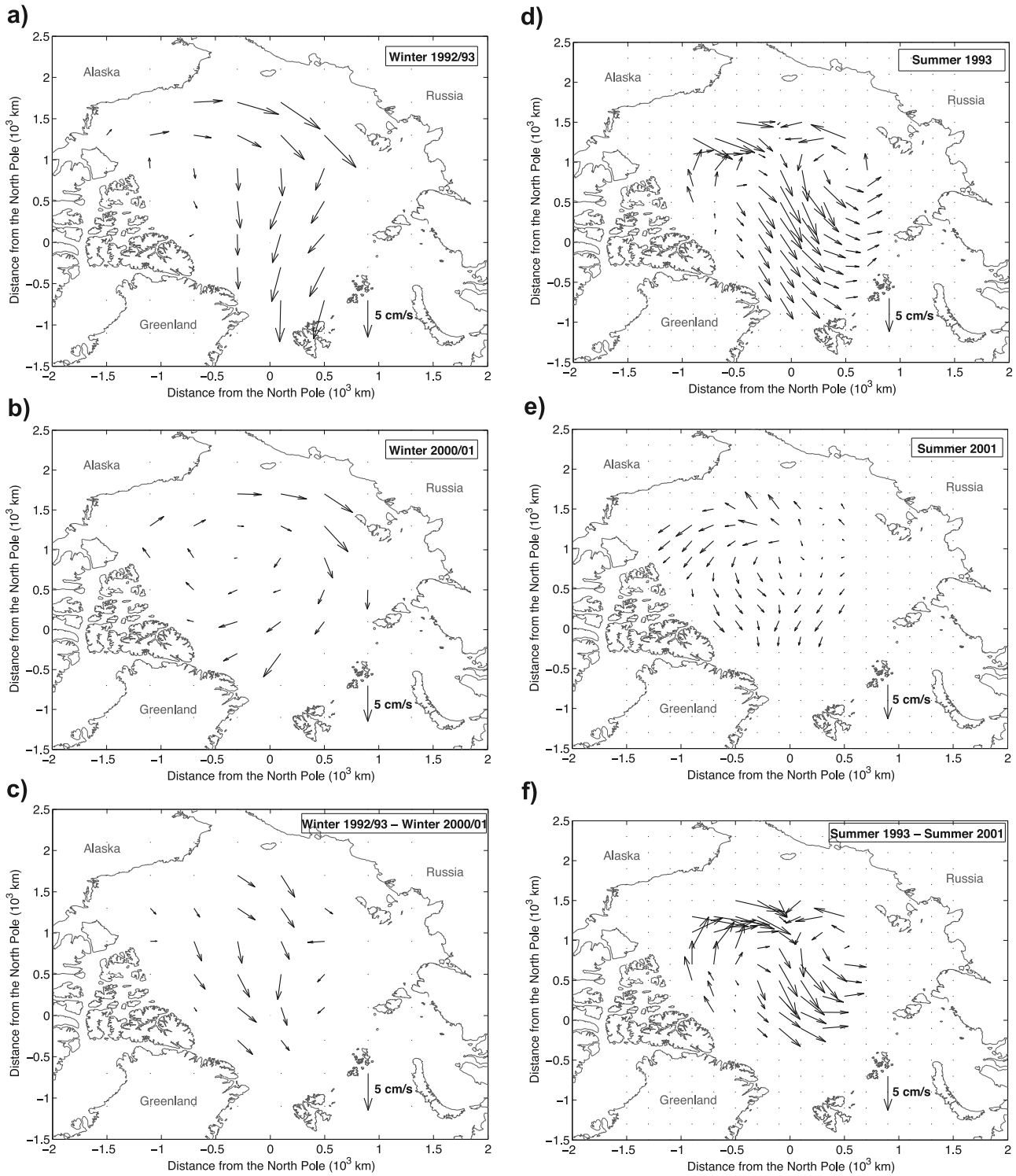

Figure 6. Interpolated mean velocity field for (a) winter 1992–1993, (b) winter 2000–2001, the difference between (c) both winters, (d) summer 1993, (e) summer 2001, and the difference between (f) both summers. The mean fields are calculated for averaging scales of 400 km and 160 days for winters and 200 km and 80 days for summers. These maps illustrate the seasonal and interannual variability of the AMGC. The maps (c) and (f) point out the fact that these variations are of the same order of magnitude than the mean speeds themselves.

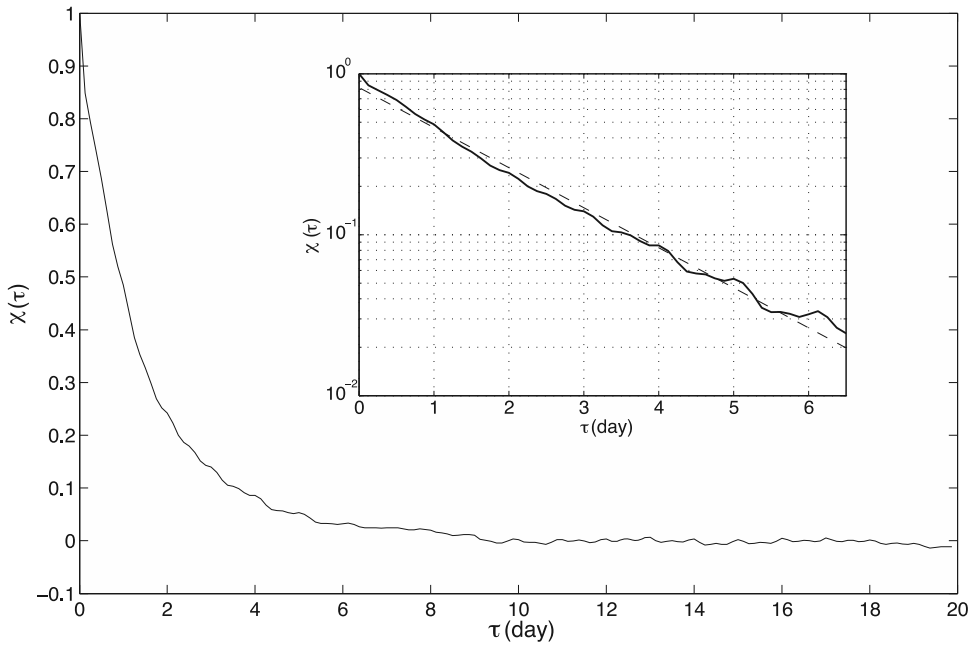

Figure 7. Averaged autocorrelation function of the sea ice fluctuating velocity for winter. The inset plot shows the time range where the autocorrelation function can be modeled by an exponential decay.

We also note that the k^{-2} scaling is the translation of the $k^{-5/3}$ scaling that holds for fluid turbulence in the Eulerian framework.

[30] We can also observe on Figure 8 that a characteristic frequency of about 2 cycles per day (i.e., a time period of 12 hours) is clearly marked by a peak in the power spectra of both seasons. This peak was observed in similar analyses of the total sea ice velocity signal and was viewed as inertial oscillations of period $T = 1/(2\omega \sin(\lambda))$ where λ is the latitude [*Hunkins*, 1967; *McPhee and Kantha*, 1989; *Colony*

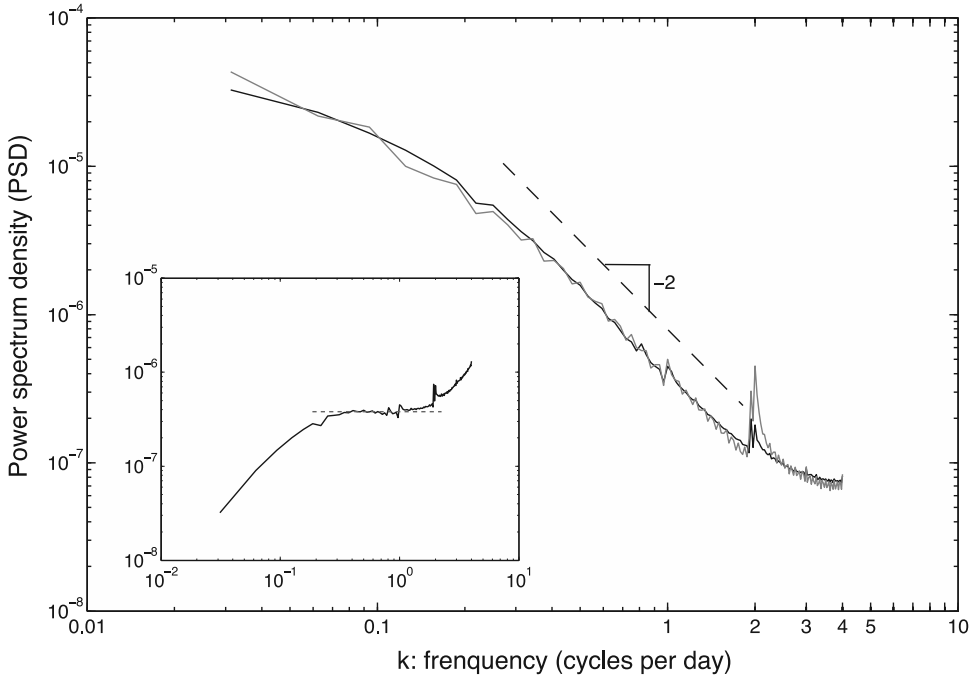

Figure 8. Power spectrum of the velocity fluctuations for winter (in black) and summer (in gray) in a log-log scale. The dashed line is for reference only and corresponds to the regime expected for a turbulent fluid by the K41 theory in the inertial range (i.e., for fully developed turbulence). The inset shows the power spectrum of winter multiplied by k^{-2}; the plateau corresponds to the range where a Kolmogorov-like scaling holds true.

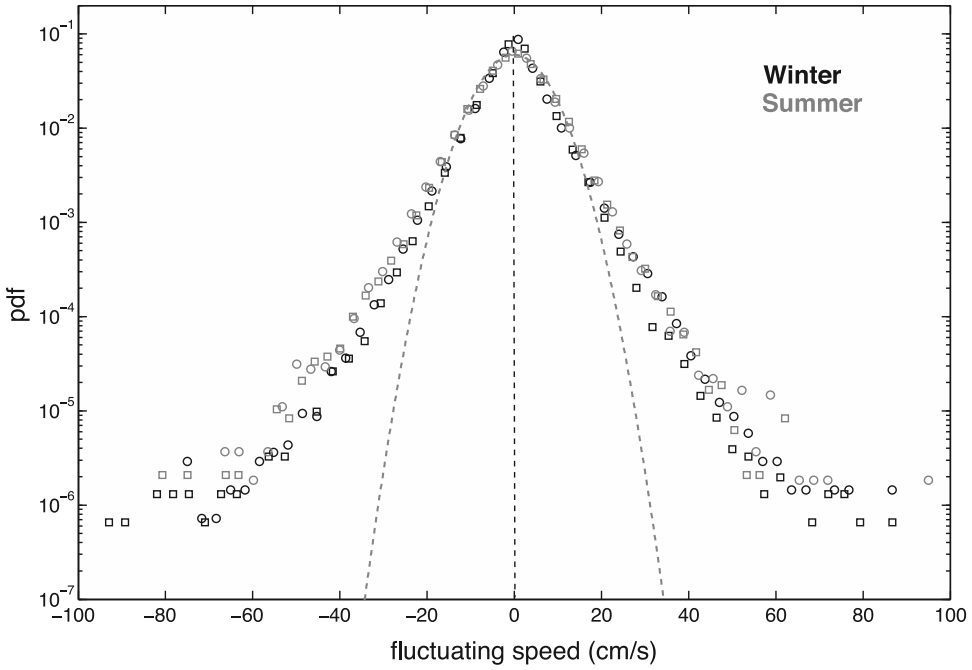

Figure 9. Probability density functions for the x and y components u_x' (circles) and u'_y (squares) of the fluctuating velocity vector $\mathbf{u}'$. Winter is in dark, and summer in gray. The means of the distributions are -0.05 cm/s (u'_x) and 0.01 cm/s (u'_y) for winter and are -0.01 cm/s (u'_x) and 0.09 cm/s (u'_y) for summer. The shapes of the PDFs are symmetrical, and the symmetry axis is drawn as a vertical dashed line. The Gaussian distribution corresponding to the winter's data (i.e., with mean and standard deviation equal to those of the distributions of u_x' and u_y' merged) is plotted as the gray dashed line.

and Thorndike, 1980; *Thorndike*, 1986b; *Heil and Hibler*, 2002]. These inertial motions are related to the surface currents of the Arctic Ocean [*McPhee*, 1978]. These do not have to be included in the random part of the sea ice motion. Indeed, the oceanic inertial oscillations are predictable in a deterministic sense. Figure 8 shows that the peak is stronger in summer than in winter. This difference at the inertial frequency could be explained by the greater percentage of open water during the summer. In summer, the motion of the less-consolidated sea ice cover is closer to the free drift hypothesis without any wind-forcing and therefore better follows the motion of the underlying ocean.

4.2. Distributions of Fluctuating Velocity

[31] Figure 9 shows the probability density functions (PDFs) of x and y components of the fluctuating velocity $\mathbf{u}'$, noted u'_x and u'_y respectively, for both seasons. The distributions of u'_x and u'_y are symmetric and centered on zero. The symmetry and the superposition of both components reflect the isotropic character of the fluctuating velocity field (see Figure 2 and section 3.2). No strong differences are observed between winter and summer. However, we here note that, as the averaging scales $\tilde{L}$ and $\tilde{T}$ are smaller for summer, the total speeds u in summer are in fact much larger than those in winter. Maximum fluctuating speeds are approximately 1 m/s, i.e., two orders of magnitude larger than the speeds of the AMGC. We also checked that the distributions of u_x and u_y (i.e., the two components of the total velocity) are neither symmetric nor centered on zero: we can interpret this as the fingerprint of the AMGC (e.g., the Transpolar Current can explain the negative mean value of the distributions of u_y). Thus the symmetry of the PDFs of u'_x and u'_y confirms that the AGCM is correctly removed by averaging at the scales $\tilde{L}$ and $\tilde{T}$. It is also in agreement with what would be obtained for fluctuating velocities in a pure turbulent flow [*Taylor*, 1921].

[32] However, our statistics deviate from this theory in the following way: We show in Figure 10 the PDF of the norm of $\mathbf{u}'$ defined as $u' = (u'^2_x + u'^2_y)^{1/2}$, merging the winter and summer speed values. The data follow an exponential distribution instead of the Gaussian distribution as expected in fully developed turbulence [*Batchelor*, 1960; *Frisch*, 1995] and observed in different turbulent fluids [*Van Atta and Chen*, 1970; *Zhang et al.*, 2001], therefore allowing fluctuating speeds much larger than a standard deviation away from the zero mean. We checked that this departure from the corresponding Gaussian distribution cannot be explained by the uncertainties on buoy positions. Indeed, this departure occurs for speed values larger than 20 cm/s (see Figure 9), i.e., much larger than the upper bound for speed errors (1.3 to 3 cm/s, see section 2). Therefore the exponential tail cannot be explained by such errors. We also checked that the distributions of both components of the total velocity $\mathbf{u}$ are exponential as well (not shown here), and interpreted as the fingerprint of the fluctuations statistics. A great challenge would be to understand the origin of this difference from turbulent flows statistics. We will discuss further this point in section 5.

[33] In conclusion, we show that the fluctuating part of sea ice velocity is characterized by zero means, symmetrical exponential distributions.

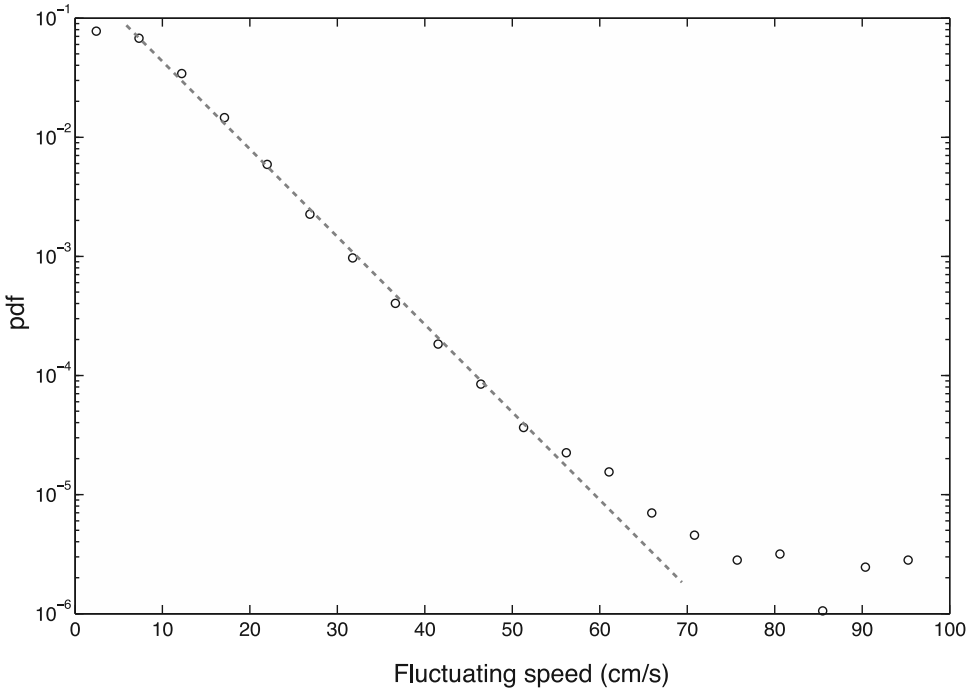

Figure 10. PDF of the fluctuating speed $u' = (u_x'^2 + u_y'^2)^{1/2}$ for the merged winter and summer data sets. The best exponential fit of the data is drawn as the gray dashed line. The slope of the exponential function allows us to estimate a characteristic speed of about 7.4 cm/s, i.e., very close to the mean value of the distribution that is about 7.8 cm/s. The few outliers above 60 cm/s can explain this small difference.

4.3. Intermittency and Scaling

[34] Here we focus our analysis on the winter season. Figure 11 shows the PDFs of the two components $\Delta_\tau u_x$ and $\Delta_\tau u_y$ of the velocity increments Δ_τ **u** for different timescales τ.

[35] The PDFs are normalized to their unit variance in order to emphasize changes in the functional forms. We can see that the PDFs are symmetric about $\Delta u = 0$, in agreement with the local symmetries in the velocity field illustrated by the lack of skewness in the PDF of the Lagrangian fluctuating velocity in winter (see Figure 9). At small τ (i.e., for τ = 3 hours), the PDFs of both components show power law tails. These could be used to determine the PDF of the Lagrangian acceleration, assumed to be approximately given by $(\Delta_\tau u/\tau)_{\tau\to 0}$ [*Frisch*, 1995]. At large τ (i.e., here for $\tau \geq$ 2 days), the PDFs become exponential and stabilize. In between these extremes, the change is continuous. The variability of the velocity increments is much stronger at short timescales (power law PDF) than what could have been expected for the larger timescales (exponential PDF).

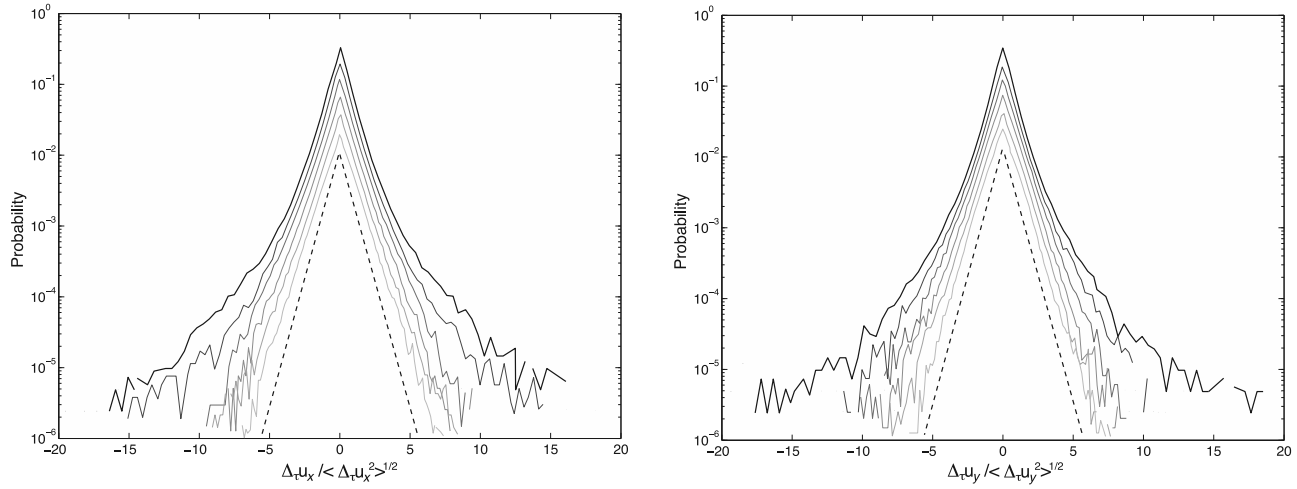

Figure 11. PDFs of the normalized increment $\Delta_\tau u/\sigma_\tau$ for the two components of the velocity vector **u**. The curves are shifted for clarity. From top to bottom: τ = [0.125, 0.25, 0.5, 1, 2, 5] days. The dashed lines show an exponential decay and are for reference only.

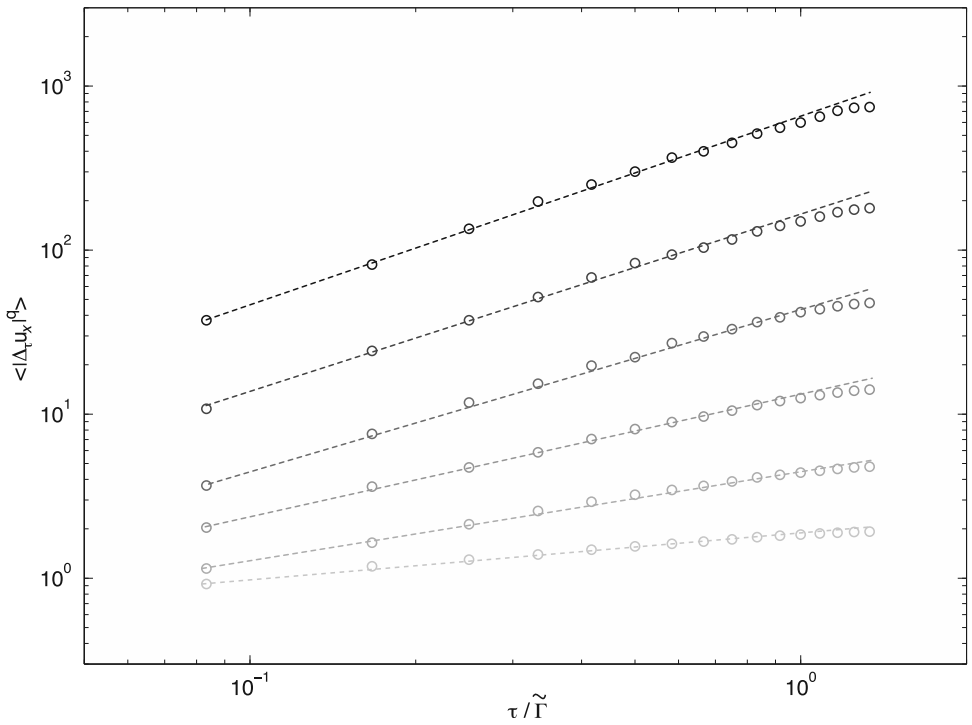

Figure 12. Lagrangian structure functions of the x component of the velocity for $q = 0.5$, 1, 1.5, 2, 2.5, and 3 for winter. The dashed lines are the least squares power law fits $\langle|\Delta_\tau u|^q\rangle \sim \tau^{\zeta(q)}$ yielding the exponents $\zeta(q)$.

This temporal "localization" of the velocity increment at short timescales is also called intermittency.

[36] In order to quantify this intermittency, we study how the PDF of the velocity increments continuously change with the timescale. This can be done by examining the dependence of the moment of order q of $|\Delta_\tau u|$ with τ. This dependence takes the form

$$\langle|\Delta_\tau u|^q\rangle \sim \tau^{\zeta(q)} \tag{17}$$

as can be seen on Figure 12. Figure 12 shows the structure function $\langle|\Delta_\tau u_x|^q\rangle$ of u_x versus τ for $q = 0.5$ to 3 by step of 0.5 along with the least squares dashed lines. A clear power law scaling (equation (17)) is observed from $\tau = 3$ hours to $\tau \approx \tilde{\Gamma}$, i.e., the so-called inertial range for turbulent flows. This scaling does no longer hold for $\tau > \tilde{\Gamma}$, as expected [*Mordant et al.*, 2003]. We checked that similar results also hold for u_y.

[37] The values of the slopes define the function $\zeta(q)$, which is shown in Figure 13. From the k^{-2} scaling of the fluctuating velocity power spectrum (Figure 8), we expect that the second order structure function $\langle|\Delta_\tau u_x|^2\rangle$ scales as τ [see, e.g., *Mordant et al.*, 2003; *Biferale et al.*, 2006]. This is in agreement with our results since we obtain $\zeta(2) = 0.95$. The nonlinearity of $\zeta(q)$ is a signature of a functional change in the PDF of u that does not amount to a simple rescaling. The exponents $\zeta(q)$ are remarkably well approximated by a quadratic fit $f(q) = aq^2 + bq$ with $a = -0.09$ and $b = 0.65$, expressing that the velocity fluctuations can be modeled by a lognormal multiplicative cascade process (see *Yaglom* [1966] for such a model in the case of three-dimensional fully turbulence). While multifractality is a well-known property of turbulent flows at high Reynolds numbers [*Mordant et al.*, 2003; *Schmitt*, 2006], it is observed here to also occur for a solid, i.e., the Arctic sea ice cover.

[38] We illustrate how the function $\zeta(q)$ indeed quantifies the intermittency of the velocity increments. The coefficient of variation cov, defined as the ratio of the standard deviation over the mean, scales with τ as

$$\mathrm{cov} \sim \frac{\left\langle|\Delta_\tau u|^2\right\rangle^{1/2}}{\langle|\Delta_\tau u|\rangle} \sim \tau^{\frac{\zeta(2)}{2}-\zeta(1)} \sim \tau^{-0.08} \tag{18}$$

and slowly grows at short timescales. This is a direct signature of the temporal localization, which is relatively mild in our case (slow divergence).

4.4. Diffusion Regimes of Sea Ice

[39] In the turbulent diffusion theory of *Taylor* [1921], the particle diffusion through time $\langle r'^2(t)\rangle$ has two asymptotic regimes (equations (6) and (7)). We check here whether these regimes exist for the Arctic sea ice. We compute the sea ice displacements r'_x and r'_y (along the x axis and y axis directions respectively) caused by the fluctuating velocity field of sea ice for winter and summer (see Figure 14). The symmetry about the zero line indicates once again the correct removal of the mean velocity structure; otherwise, the displacements would be biased toward one direction [*Riser and Rossby*, 1983]. The envelope of the drifter trajectories grows more quickly at the beginning and then slows down, qualitatively following the Taylor diffusion theory. To quantify this, we plot for winter and summer the variance of r', defined as $\langle r'^2(t)\rangle = \langle r'^2_x(t) + r'^2_y(t)\rangle$, versus

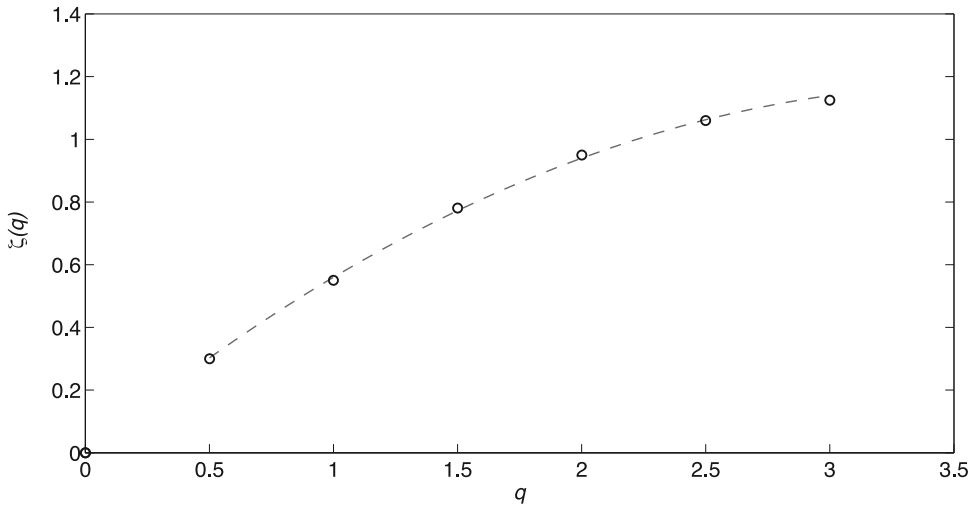

Figure 13. Functions $\zeta(q)$ versus moment order q (open circles) and the best fit quadratic curve (dashed line).

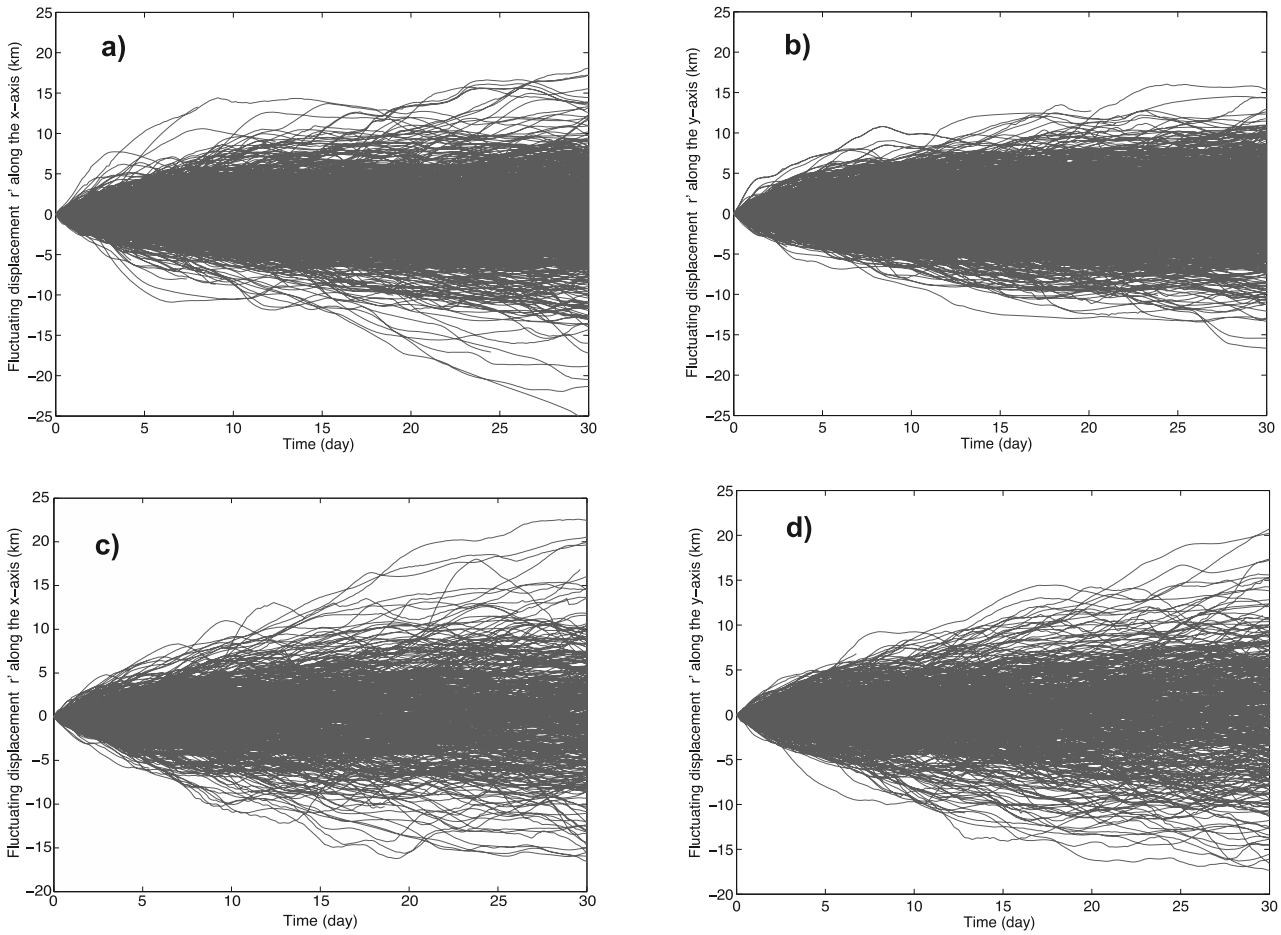

Figure 14. Particle displacements r_x' (along x) and r_y' (along y) caused by the fluctuating velocity field for (a and b) winter and (c and d) summer. The fluctuating displacements are calculated from buoy tracks for which the displacement associated with the mean flow is removed. After 30 days, fluctuating displacements are, on average, stronger in summer than in winter.

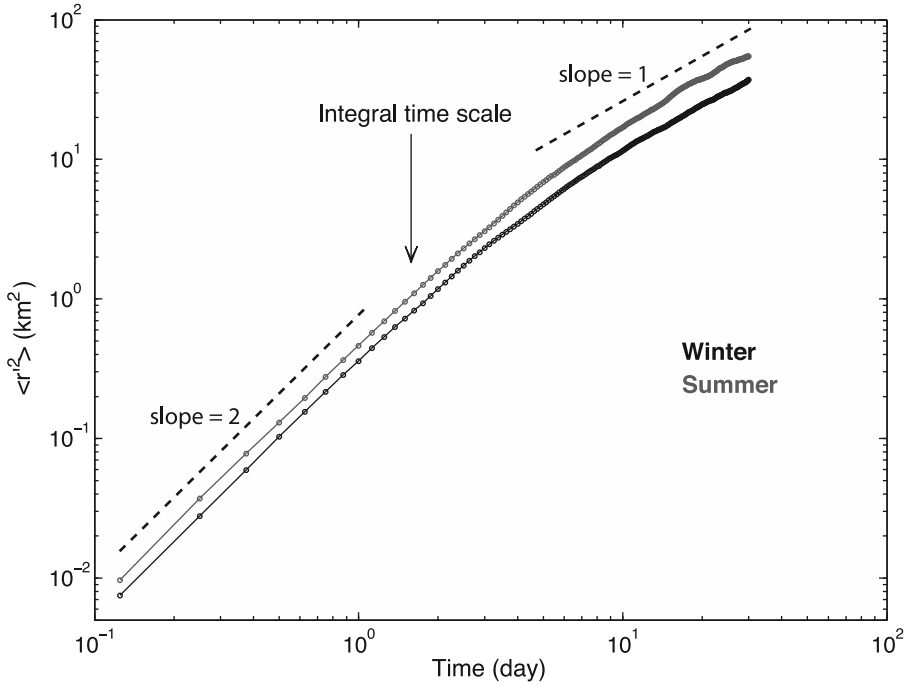

Figure 15. Plot of the variance $\langle r'^2 \rangle$ of the fluctuating displacement r' versus time in log-log scale. The fluctuating displacement is defined as $r' = (r_x'^2 + r_y'^2)^{1/2}$. The dashed lines show the two regimes expected by the Taylor diffusion theory, i.e., for the initial ballistic regime ($t \ll \Gamma$) and long-time random walk ($t \gg \Gamma$). We also show in the plot the integral time value estimated previously from the Lagrangian autocorrelation functions.

time on a log-log scale (see Figure 15). We see that the fluctuating part of the sea ice motion follows the Taylor diffusion for both seasons and is consistent with our results presented in section 3 obtained by an analysis of the autocorrelation function: at time $t \ll \tilde{\Gamma}$ (around 1.5 and 1.3 days for winter and summer, respectively) the displacement variance grows with t^2; at $t \gg \tilde{\Gamma}$ (i.e., $t > 10$ days), it grows with t. The regime for which displacement variance grows with t was expected since we showed in section 4.2 that the distribution of the fluctuating speed of sea ice is exponential. Indeed, exponential distributions are in the Gaussian attractive basin (by addition of independent variables [*Bouchaud and Georges*, 1990; *Sornette*, 2000]) and then lead to the same diffusive regime for times larger than the integral timescale $\tilde{\Gamma}$.

[40] We also computed a turbulent-like diffusivity of the Arctic sea ice following equation (10) for $t \gg \tau$. We found a diffusivity of about 0.44×10^3 m^2/s for winter and about 0.45×10^3 m^2/s for summer. These values lie in the range of diffusivities estimated for the surface of the open ocean (i.e., between 0.025 and 0.66×10^3 m^2/s) [*Colin de Verdière*, 1983; *Krauss and Böning*, 1987; *Poulain et al.*, 1996].

[41] We found in section 3 that the integral time Γ for sea ice is about 1.5 days in winter and 1.3 days in summer. For the ocean surface, Γ values were reported by several studies in which analyses of drifting buoys trajectories are performed [*Colin de Verdière*, 1983; *Krauss and Käse*, 1984; *Davis*, 1985; *Krauss and Böning*, 1987; *Poulain and Niiler*, 1989; *Poulain et al.*, 1996]: Integral times range from 1 day to 4.5 days, depending on the location (i.e., near coasts, or in the open ocean), i.e., these estimates are of the same order of those obtained in this study. For comparison, our estimates are five orders of magnitude larger than typical integral time estimated from Lagrangian velocities of neutral balloons moving in the boundary layer of the atmosphere at altitudes between 100 and 300 m [*Hanna*, 1980].

4.5. Discussion

[42] A comparison of the diffusion properties of buoys anchored to the sea ice cover (e.g., the IABP buoys) in one hand, and buoys floating at the surface of the ocean in another hand (see, e.g., *Zhang et al.* [2001]), reveals several similarities:

[43] 1. The inertial oscillation frequency appears in the velocity power spectra;

[44] 2. The same diffusion regimes apply, as derived from the turbulent diffusion theory of *Taylor* [1921];

[45] 3. The integral time and diffusivity are of the same order of magnitude.

[46] However, we showed in section 4.2 that the distribution of the IABP buoys speeds are strongly different from those observed for oceanic drifters [see, e.g., *Zhang et al.*, 2001], i.e., exponential instead of Gaussian. Which cause can explain, or at least contribute, to this difference?

[47] The motion of surface oceanic drifters is guided by the upper ocean currents that are themselves the mechanical response of the surface waters to the wind-forcing, and characterized by Gaussian velocities. The mechanical response of the ice pack, a solid body, to the atmospheric forcing is not the same than the one of the ocean: In the case of the ocean, the atmospheric forcing generates pressure gradients, which in turn are responsible for the surface currents. The sea ice cover responds to the atmospheric

forcing and the boundary conditions of the Arctic basin through internal stresses (mostly shear but also tension and compression). The deformation of the Arctic sea ice cover results from these stresses. As shown recently, most of the sea ice deformation is accommodated by a multiscale fracturing and faulting process [*Weiss et al.*, 2009, 2007] leading to strong spatial heterogeneity and intermittency of the strain rates [*Marsan et al.*, 2004; *Rampal et al.*, 2008]. Intermittency of internal stress amplitudes [*Weiss and Marsan*, 2004] and principal stress directions [*Weiss*, 2008] were revealed from a multifractal analysis. The intermittency of principal stress directions within sea ice is much more pronounced than that of wind direction. The similarity between the intermittency of stress amplitudes in the one hand, and sea ice velocity increments as seen in section 4.3 of this study in the other hand, suggests that the particular mechanical response of the sea ice cover plays a significant role in the statistical properties of sea ice kinematics and dynamics.

[48] From a more general point of view, we remark that the Arctic sea ice diffusion, i.e., single particle statistics, does not differ strongly from those of turbulent fluids, excepting for velocity distributions and intermittency. Therefore mean velocity fields and diffusion properties are probably not a discriminating factor to test sea ice models. On another hand, *Rampal et al.* [2008] showed that the Arctic sea ice dispersion, i.e., pair particle statistics (which can be linked to the sea ice deformation statistics), strongly differs from those of fluid parcels in turbulent flows. Thus our results indicate that the evaluation of models on the basis of a correlation analysis between the observed and the modeled mean velocity fields (i.e., a comparison at the first order in space) is, taken alone, not sufficient. A more thorough evaluation of models would be to compare the displacements fields at the second order, i.e., the deformation fields. So far, these are poorly described by models [*Thomas*, 1999; *Lindsay et al.*, 2003], especially the linear-like structures of localized deformation observed at all scales and which correspond to active faults [see, e.g., *Weiss et al.*, 2007]. Such evaluation of sea ice models should be done using a space-time analysis similar to that presented by *Rampal et al.* [2008] and *Girard et al.* [2009].

5. Conclusions

[49] The main conclusions of this study are:

[50] 1. The Arctic sea ice velocity field can be partitioned into a mean field and a fluctuating field using an approach inspired from the study of fluid turbulence. In order to study the fluctuating velocity field, one has to consider separately the summer and winter seasons, and subtract from the total velocity field a mean field estimated at averaging scales of about $L = 400$ km and $T = 5\ ^1/_2$ months in winter, or $L = 200$ km and $T = 2\ ^1/_2$ months in summer.

[51] 2. Estimated at these scales, the seasonal mean field shows a strong interannual variability, excepting the Transpolar current that is always observed all years long.

[52] 3. Once extracted from the total velocity field, the fluctuating field can be studied within the framework of the turbulent diffusion theory of *Taylor* [1921]. Performing an analysis of the fluctuating velocity field properties, we show that sea ice diffusion follows the same diffusive regimes than those of turbulent flows, and that the integral time and diffusivity of sea ice are of the same orders than those of the upper ocean.

[53] 4. The fluctuating speed distributions differ from those of homogenous and isotropic turbulence as they show an exponential decay.

[54] 5. The analysis of sea ice velocity increments reveals a multifractal scaling, expressing the intermittency of sea ice velocity, which progressively changes from an exponential (at times larger than a few days) to a power law distribution at short times (down to 3 hours).

[55] 6. The oceanic and atmospheric dynamic forcing cannot explain solely the statistical properties of sea ice kinematics and dynamics. We argue that sea ice dynamic is significantly influenced by the interplay of multiple fractures that are activated intermittently within the ice pack.

[56] **Acknowledgments.** We thank I. Rigor from the Polar Science Centre of Seattle and O. Persson from the Earth Observing Laboratory of the NCAR for the compilation and the distribution on the Web of the IABP data set and the wind speed data set of SHEBA, respectively.

References

Batchelor, G. K. (1960), *The Theory of Homogeneous Turbulence*, 197 pp., Cambridge Univ. Press, Cambridge, U. K.

Bauer, S., M. S. Swenson, A. Griffa, A. J. Mariano, and K. Owens (1998), Eddy-mean flow decomposition and eddy-diffusivity estimates in the Tropical Pacific Ocean: 1. Methodology, *J. Geophys. Res.*, *103*(C13), 30,855–30,871.

Biferale, L., G. Boffeta, A. Celani, A. Lanotte, and F. Toschi (2006), Lagrangian statistics in fully developed turbulence, *J. Turb.*, *7*(6).

Bouchaud, J. P., and A. Georges (1990), Anomalous diffusion in disordered media, *Phys. Rep.*, *195*, 127.

Bourgoin, M., N. T. Ouellette, H. Xu, J. Berg, and E. Bodenschatz (2006), The role of pair dispersion in turbulent flow, *Science*, *311*, 835–838.

Colin de Verdière, A. (1983), Lagrangian eddy statistics from surface drifters in the eastern North Atlantic, *J. Mar. Res.*, *41*, 375–398.

Colony, R., and A. S. Thorndike (1980), The horizontal coherency of the motion of summer Arctic sea ice, *J. Phys. Ocean.*, *10*(8), 1281–1289.

Colony, R., and A. S. Thorndike (1984), An estimate of the mean field of Arctic sea ice motion, *J. Geophys. Res.*, *89*(C6), 10,623–10,629.

Davis, R. E. (1985), Drifter observations of coastal Surface currents during CODE: The statistical and dynamical views, *J. Geophys. Res.*, *90*(C3), 4756–4772.

Deser, C., and H. Teng (2008), Evolution of Arctic sea ice concentration trends and the role of atmospheric circulation forcing, *Geophys. Res. Lett.*, *35*, L02504, doi:10.1029/2007GL032023.

Figueroa, H. A., and D. B. Olson (1994), Eddy resolution versus eddy diffusion in a double gyre GCM: Part I. The Lagrangian and Eulerian description, *J. Phys. Oceanogr.*, *24*, 371–386.

Freeland, H. J., P. B. Rhines, and T. Rossby (1975), Statistical observations of the trajectories of neutrally buoyant floats in the North Atlantic, *J. Mar. Res.*, *33*, 383–404.

Frisch, U. (1995), *Turbulence: The Legacy of A.N Kolmogorov*, Cambridge Univ. Press, Cambridge, U. K.

Gandin, L. S. (1963), Objective analysis of meteorological field, 286 pp., Gidrometeorologich eskoe Izdatel'sivo., Leningrad, U.S.S.R.

Gifford, F. (1955), A simultaneous Lagrangian-Eulerian turbulence experiment, *Mon. Weather Rev., 83*, *12*, 293–301.

Girard, L., J. Weiss, J. M. Molines, B. Barnier, and S. Bouillon (2009), Evaluation of high-resolution sea ice models on the basis of statistical and scaling properties of Arctic sea ice drift and deformation, *J. Geophys. Res.*, *114*, C08015, doi:10.1029/2008JC005182.

Hanna, S. R. (1980), Lagrangian and Eulerian time-scale relations in the daytime boundary layer, *J. Appl. Meteorol.*, *20*, 242–249.

Hay, J. S., and F. Pasquill (1959), Diffusion from a continuous source in relation to the spectrum and scale of turbulence, *Adv. Geophys.*, *6*, 345–365, Academic Press.

Haynes, R., and E. D. Barton (1991), Lagrangian observations in the Iberian coastal transition zone, *J. Geophys. Res.*, *96*(C8), 14,731–14,741.

Heil, P., and W. D. Hibler (2002), Modeling the high-frequency component of Arctic sea ice drift and deformation, *J. Phys. Oceanogr.*, *32*, 3039–3057.

Hunkins, K. (1967), Some inertial oscillations of Fletcher's Ice Island, *J. Geophys. Res.*, *72*(4), 1165–1174.

Hurrell, J. W. (1995), Decadal trends in the North Atlantic Oscillation: Regional temperatures and precipitation, *Science*, *269*, 676–679.

Krauss, W., and R. H. Käse (1984), Mean circulation and eddy kinetic energy in the eastern North Atlantic, *J. Geophys. Res.*, *89*(C3), 3407–3415.

Krauss, W., and C. W. Böning (1987), Lagrangian properties of eddy fields in the northern North Atlantic as deduced from satellite-tracked buoys, *J. Mar. Res.*, *45*, 259–291.

Lien, R.-C., E. A. D'Asaro, and G. T. Dairiki (1998), Lagrangian frequency spectra of vertical velocity and vorticity in high-Reynolds-number oceanic turbulence, *J. Fluid Mech.*, *362*, 177–198.

Lindsay, R. W., J. Zhang, and D. A. Rothrock (2003), Sea-ice deformation rates from satellite measurements and in a model, *Atmos. Ocean*, *41*(1), 35–47.

McPhee, M. G. (1978), A simulation of inertial oscillations in drifting pack ice, *Dyn. Atmos. Oceans*, *2*, 107–122.

McPhee, M. G., and L. H. Kantha (1989), Generation of internal waves by sea ice, *J. Geophys. Res.*, *94*(C3), 3287–3302.

Marsan, D., J. Weiss, R. Lindsay, and H. Stern (2004), Scale dependence and localization of the deformation of Arctic sea ice, *Phys. Rev. Lett.*, *93*, 17.

Martins, C. S., M. Hamann, and A. F. G. Fiuza (2002), Surface circulation in the Eastern North Atlantic from drifters and altimetry, *J. Geophys. Res.*, *107*(C12), 3217, doi:10.1029/2000JC000345.

Mordant, N., J. Delour, E. Léveque, O. Michel, A. Arnéodo, and J.-F. Pinton (2003), Lagrangian velocity fluctuations in fully developed turbulence: Scaling, intermittency, and dynamics, *J. Stat. Phys.*, *113*, 701–717.

Overland, J. E., M. C. Spillane, D. B. Percival, M. Wang, and H. Mojfeld (2004), Seasonal and regional variation of pan-Arctic surface air temperature over the instrumental record, *J. Clim.*, *17*(17), 3263–3282.

Poulain, P.-M., and P. P. Niiler (1989), Statistical Analysis of the surface circulation in the California current system using satellite-tracked drifters, *J. Phys. Ocean.*, *19*, 1588–1603.

Poulain, P.-M., A. Warn-Varnas, and P. P. Niiler (1996), Near-surface circulation of the Nordic seas as measured by Lagrangian drifters, *J. Geophys. Res.*, *101*(C8), 18,237–18,258.

Rampal, P., J. Weiss, D. Marsan, R. Lindsay, and H. Stern (2008), Scaling properties of sea ice deformation from buoy dispersion analysis, *J. Geophys. Res.*, *113*, C03002, doi:10.1029/2007JC004143.

Rigor, I., R. Colony, and S. Martin (2000), Variations in surface air temperature observations in the Arctic, 1979–1997, *J. Clim.*, *13*(5), 896–914.

Riser, S. C., and H. T. Rossby (1983), Quasi-Lagrangian structure and variability of the subtropical western North Atlantic circulation, *J. Mar. Res.*, *41*, 127–162.

Sawford, B. L. (1991), Reynolds number effects in Lagrangian stochastic model of turbulent dispersion, *Phys. Fluids A*, *3*(6), 1577–1586.

Schmitt, F. (2006), Linking Eulerian and Lagrangian structure function's scaling exponents in turbulence, *Phys. A*, *368*, 2.

Sornette, D. (2000), *Critical Phenomena in Natural Sciences, Springer Series in Synergetics*, Springer, Berlin.

Spall, M. A., P. L. Richardson, and J. Price (1993), Advection and eddy mixing in the Mediterranean salt tongue, *J. Mar. Res.*, *51*, 797–818.

Sundermeyer, M. A., and J. F. Price (1998), Lateral mixing and the North Atlantic tracer release experiment: Observations and numerical simulations of Lagrangian particles and a passive tracer, *J. Geophys. Res.*, *103*(C10), 21,481–21,497.

Taylor, G. I. (1921), Diffusion by continuous movements, *Proc. London Math. Soc.*, (20), Ser. 2.

Thomas, D. (1999), The quality of sea ice velocity estimates, *J. Geophys. Res.*, *104*(C6), 13,627–13,655.

Thompson, D. W. J., and J. M. Wallace (1998), The Arctic Oscillation signature in the wintertime geopotential height and temperature fields, *Geophys. Res. Lett.*, *25*(9), 1297–1300.

Thorndike, A. S., and R. Colony (1982), Sea ice motion in response to geostrophic winds, *J. Geophys. Res.*, *87*(C8), 5845–5852.

Thorndike, A. S. (1986a), Diffusion of Sea ice, *J. Geophys. Res.*, *91*(C6), 7691–7696.

Thorndike, A. S. (1986b), Kinematics of sea ice, in *The Geophysics of Sea Ice*, *NATO ASI Ser.*, vol. 146, edited by N. Untersteiner, pp. 489–549, Plenum, New York.

Van Atta, C. W., and W. Y. Chen (1970), Structure functions of turbulence in the atmospheric boundary layer over the ocean, *J. Fluid Mech.*, *44*, 145–159.

Voth, G. A., K. Satyanarayan, and E. Bodenschatz (1998), Lagrangian acceleration measurements at large Reynolds numbers, *Phys. Fluids*, *10*, 2268.

Weiss, J. (2008), Intermittency of principal stress directions within Arctic sea ice, *Phys. Rev. Lett. E*, *77*, doi:101103/PhysRevE.77.056101.

Weiss, J., and D. Marsan (2004), Scale properties of sea ice deformation and fracturing, *C. R. Phys.*, *5*, 735–751.

Weiss, J., E. M. Schulson, and H. L. Stern (2007), Sea ice rheology from in-situ, satellite and laboratory observations: Fracture and friction, *Earth Planet. Sci. Lett.*, *255*, 1–8.

Weiss, J., D. Marsan, and P. Rampal (2009), Space and time scaling laws induced by the multiscale fracturing of the Arctic sea ice cover, in *IUTAM Symposium on Scaling in Solid Mechanics*, edited by F. Borodich, pp. 101–109, Springer, New York.

Yaglom, A. M. (1966), The influence on the fluctuation in energy dissipation on the shape of turbulent characteristics in the inertial interval, *Sov. Phys. Dokl.*, *2*, 26.

Zhang, H.-M., M. D. Prater, and T. Rossby (2001), Isopycnal lagrangian statistics from the North Atlantic Current RAFOS float observations, *J. Geophys. Res.*, *106*(C7), 13,817–13,836.

M. Bourgoin, Laboratoire des Ecoulements Géophysiques et Industriels, CNRS, Université Joseph Fourier et Institut National Polytechnique de Grenoble, BP 53, F-38041 Grenoble Cedex 9, France.

D. Marsan, Laboratoire de Géophysique Interne et Tectonophysique, UMR CNRS 5559, Université de Savoie, F-73376 Le Bourget du Lac, France.

P. Rampal and J. Weiss, Laboratoire de Glaciologie et Géophysique de l'Environnement, CNRS, Université Joseph Fourier, 54, Rue Molière, F-38402 Saint Martin d'Hères, France. (prampal@lgge.obs.ujf-grenoble.fr)